Supporting Information

Distinctive Performance of Gemini Surfactant in the Preparation of Hierarchically Porous carbons via High Internal Phase Emulsion Template

Yulai Zhao, Zhuang Zhao, Jing Zhang, Mengzhi Wei, Longqiang Xiao, Linxi Hou*

Department of Materials-Oriented Chemical Engineering, College of Chemical Engineering, Fuzhou University, Fuzhou 350116, China.

Pages: 7 (including cover page); Figures: 9; Tables: 1

Table S1. Chemical formulas for the preparation of polyHIPEs

Samples	Water phase (external phase)		Oil phase (Internal phase)
	Emulsifiers	Resorcinol-formaldehyde solution	Liquid paraffin
SDLC-1.5	SDLC,0.15 g	10 g	30 g
SDLC-3	SDLC,0.3 g	10 g	30 g
SDLC-5	SDLC,0.5 g	10 g	30 g
TW20-1.5	Tween, 0.15 g	10 g	30 g
TW20-3	Tween, 0.3 g	10 g	30 g
TW20-5	Tween, 0.5 g	10 g	30 g
CTAB-1.5	CTAB, 0.15 g	10 g	30 g
CTAB-3	CTAB, 0.3 g	10 g	30 g
CTAB-5	CTAB, 0.5 g	10 g	30 g

[a] Resorcinol-formaldehyde precursor solutions consist of formaldehyde, resorcinol and sodium carbonate with a molar ratio of 2:1:0.002 in deionized water.

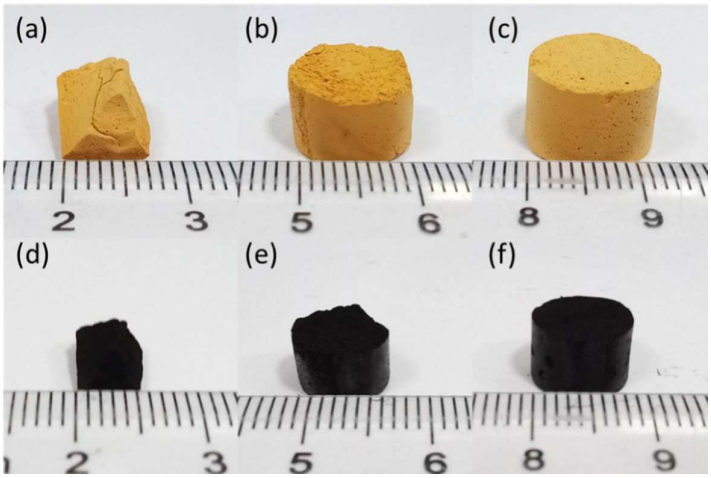

Figure S1. Photographs of polyHIPEs before (a~c) and after pyrolysis (d~f) obtained using different SDLC concentrations: (a, d) 1.5wt%, (b, e) 3wt% and (c, f) 5wt%.

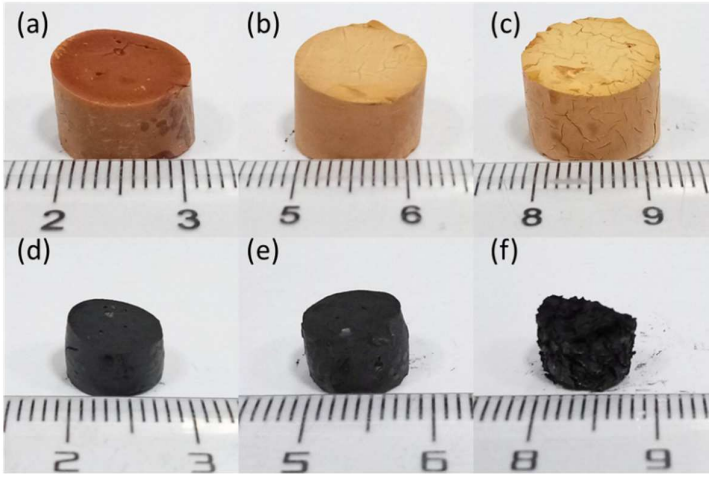

Figure S2. Photographs of polyHIPEs before (a~c) and after pyrolysis (d~f) obtained using different tween-20 concentrations: (a, d) 1.5wt%, (b, e) 3wt% and (c, f) 5wt%.

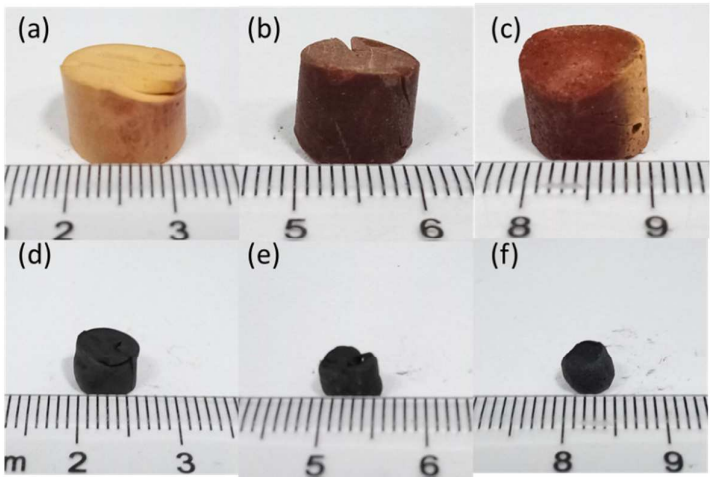

Figure S3. Photographs of polyHIPEs before (a~c) and after pyrolysis (d~f) obtained using different CTAB concentrations: (a, d) 1.5wt%, (b, e) 3wt% and (c, f) 5wt%.

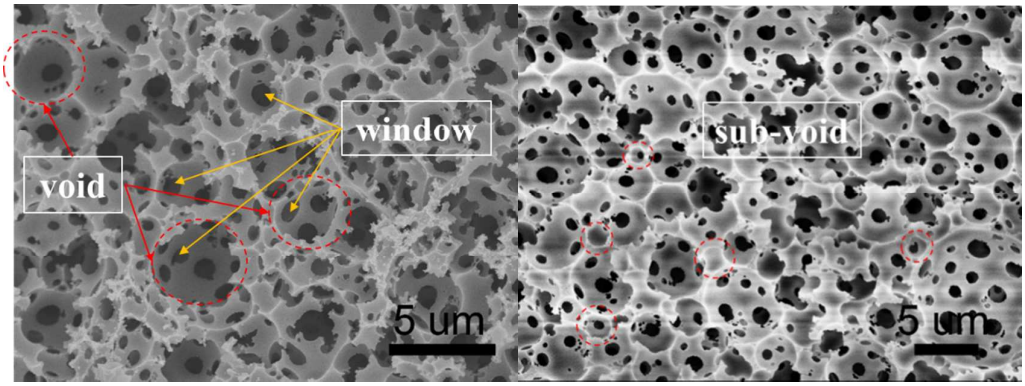

Figure S4. Illustration of the void, sub-void and window structures of polyHIPEs.

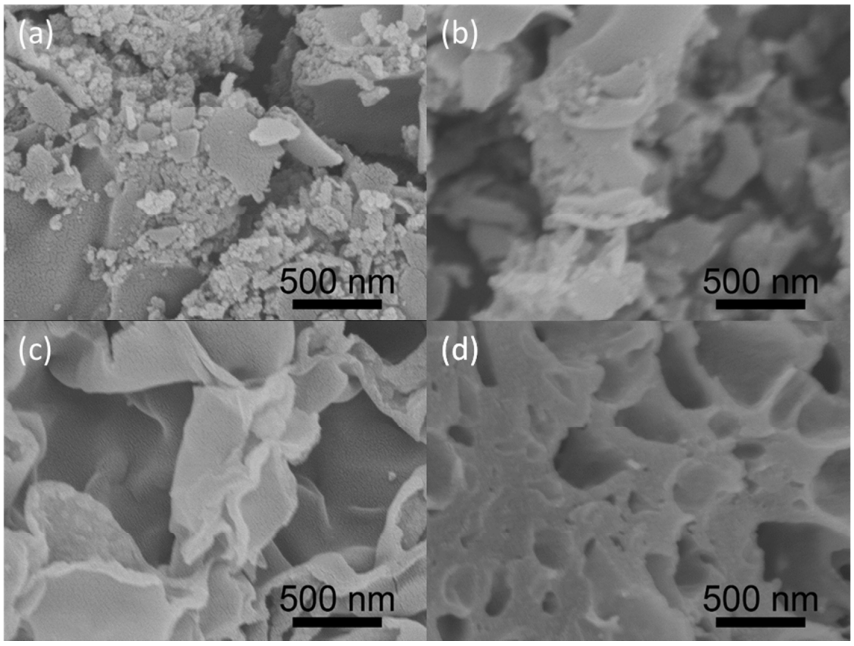

Figure S5. High resolution SEM images of carboHIPEs obtained using different emulsifiers: (a) 1.5 wt% TW20, (b) 3 wt% TW20, (c) 1.5 wt% CTAB and (d) 3 wt% CTAB.

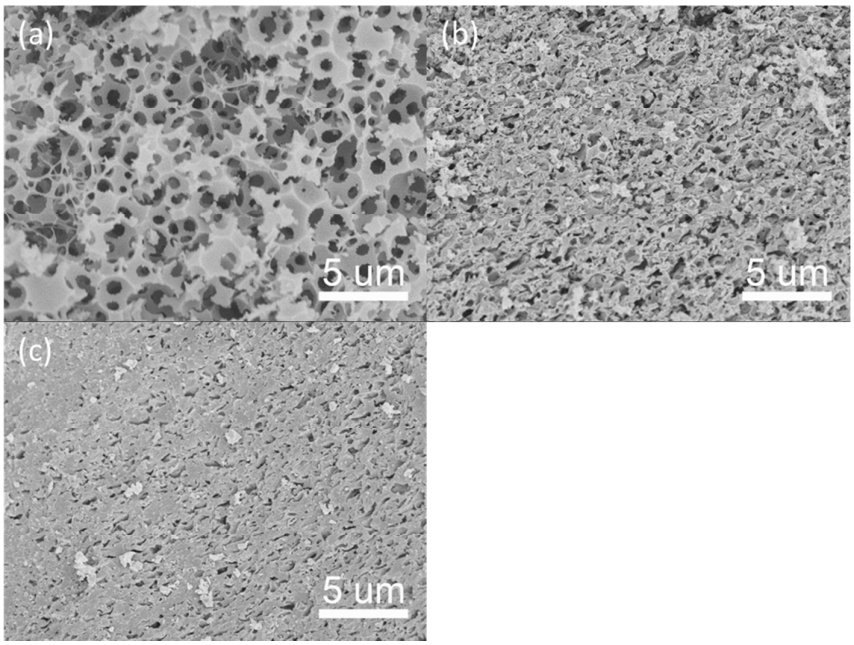

Figure S6. SEM images of activated carboHIPEs: (a) SDLC-5AC, (b) TW20-5AC and (c) CTAB-5AC.

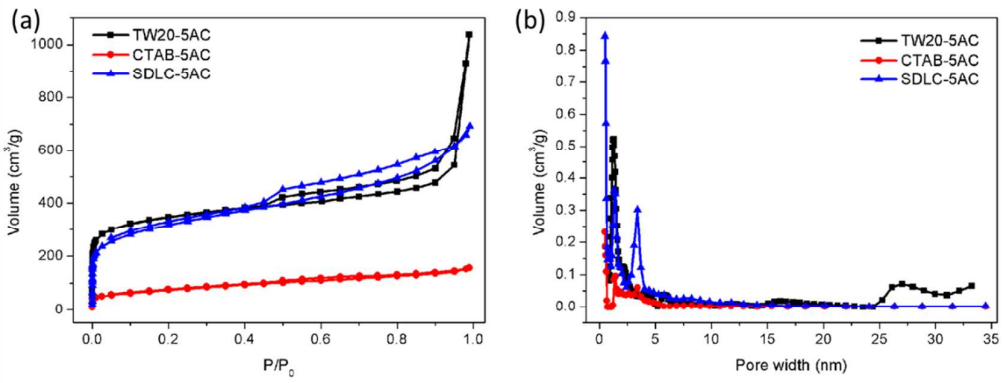

Figure S7. (a) N_2 adsorption/desorption isotherms and (b) pore size distributions of TW20-5AC, CTAB-5AC and SDLC-5AC.

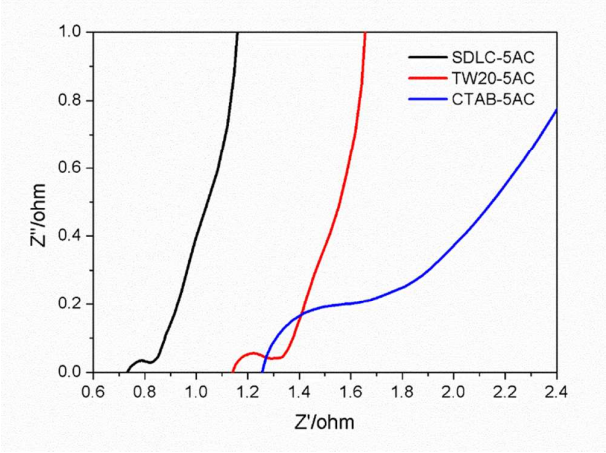

Figure S8. Nyquist plots of TW20-5AC, CTAB-5AC and SDLC-5AC.

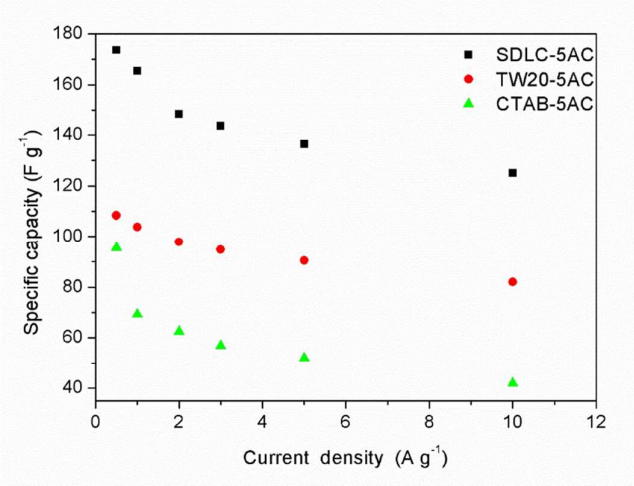

Figure S9. Dependences of specific capacitances on the current densities of TW20-5AC, CTAB-5AC and SDLC-5AC.